Time-Resolved PIV Measurement on Turbulent Wake Flow over Critical Reynolds Number for CO_2 Ocean Sequestration

by

S. Tsushima[(1)], R. Muraoka[(2)] and S. Hirai[(3)]

Tokyo Institute of Technology

Research Center for Carbon Recycling and Energy

2-12-1, Ohokayama, Meguro-ku, Tokyo, 152-8552; Japan

[(1)]E-Mail: tsushima@mech.titech.ac.jp

[(2)]E-Mail: rmuraoka@tanso.mes.titech.ac.jp

[(3)]E-Mail: hirai@tanso.mes.titech.ac.jp

ABSTRACT

CO_2 ocean sequestration is considered to be an effective global warming countermeasure. In CO_2 ocean sequestration, dilution process of injected CO_2 plays an important roll on biological impact. In this study, we investigated a turbulent wake flow behind a circular cylinder at Reynolds number(Re)=5x10^5, which simulates the wake flow behind the CO_2 releasing pipe in CO_2 ocean sequestration. By using time-resolved particle image velocimetry (PIV), we examined flow behaviour as well as turbulent properties of the wake flow over the critical Reynolds number. Figure 1a) shows a snapshot of measured two-dimensional velocity field at Re=5x10^5. In the figure, the result at Re=6x10^4 (Fig.1b)) is also displayed for comparison. Wake width at Re=5x10^5 is narrower than that at Re=6x10^4. It was also revealed that turbulent intensities normalised by mean flow velocity in case of the flow at Re=5x10^5 was about one-half to the flow at Re=6x10^4. At Re=5x10^5, vortex marching was limited in narrow region behind the wake and vortex size was small compared to that at Re=6x10^4. Thus, turbulent motion in the wake was restricted in the case of the high Reynolds number flow. This leads to reduction of wake width and turbulent intensities in the wake flow over critical Reynolds number.

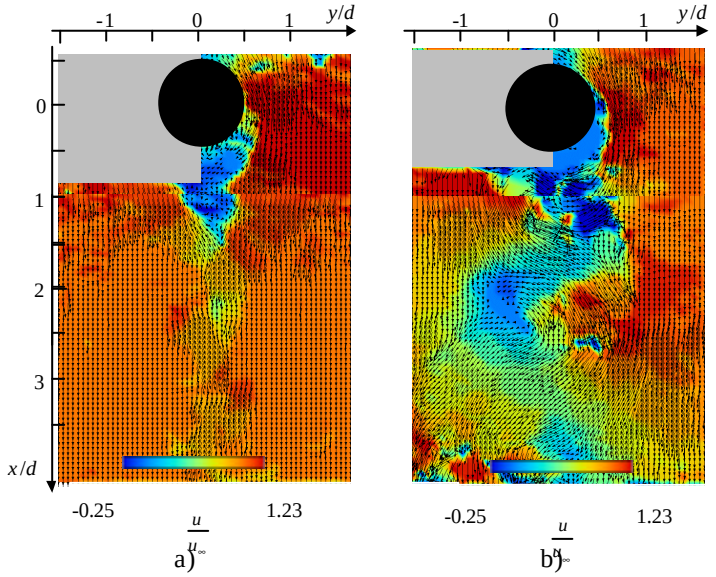

Fig. 1. Two-dimensional velocity distributions of the wake flow measured by PIV
a) Re=5x10^5 (the wake flow over the critical Reynolds number)
b) Re=6x10^4 (the wake flow under the critical Reynolds number)

1. INTRODUCTION

CO_2 ocean sequestration, proposed by Marchtti, 1977, is considered to be an effective global warming countermeasure. One of CO_2 ocean sequestration method is releasing liquid CO_2 droplets from a releasing pipe in intermediate depth of ocean, which leads to direct dissolution of CO_2 in seawater (Murai, et al., 2003). For enhancement of CO_2 dilution process to lower biological impact, a method to make use of entrainment of a wake flow behind the CO_2 releasing pipe and/or a turbulent generator attached to the pipe has been recently considered.

To discuss implementation of this method, it is necessary to evaluate dissolution process of CO_2 in seawater. Released liquid CO_2 droplets from the pipe are dispersed into the sea vertically due to buoyancy effect (Liro, et al., 1992, Morishita, et al., 1993) and horizontally due to turbulent mixing behind the pipe and/or the turbulent generator. Thus, turbulent mixing in the wake flow plays a key role on horizontal dispersion of released CO_2 (Cheng, et al., 2003).

The turbulent wake flow in CO_2 ocean sequestration is to be over the critical Reynolds number. Reynolds number of the wake flow is about $6x10^5$ when the speed of a ship and the pipe diameter are assumed to be 3 m/s and 0.3 m, respectively. It is well known that the turbulent wake flow over the critical Reynolds number (Re=$3.5x10^5$) shows its own characteristic as drag coefficient sharply decreases in the range over the critical Reynolds number. However, its flow characteristics and turbulent properties that are vital for reliable prediction of CO_2 dispersion are not fully clarified in detail. Therefore, it is important to elucidate turbulent flow fields over the critical Reynolds number for implementation of releasing CO_2 into the ocean. However, it is by no means of ease to construct an experimental apparatus for investigation on such a high Reynolds flow precisely, because of its handling and maintenance.

In the present study, we constructed a laboratory-scaled experimental apparatus to carry out a high Reynolds number flow, Reynolds number of which was about $5x10^5$, to obtain fundamental understanding on turbulent flow behaviour behind a circular cylinder. Furthermore, we also measured statistical turbulent properties useful for numerical simulation by applying time-resolved particle image velocimetry (PIV).

We also conducted experiments on an intermediate Reynolds number flow to compare with the high Reynolds number flow. The intermediate Reynolds number flow (Re=$6x10^4$) less than the critical Reynolds number was also realised on the same experimental facility in an effort to illuminate its distinctive nature of turbulent flow characteristics over the critical Reynolds number.

2. EXPERIMENTAL METHOD and PROCEDURES

2.1 Experimental Apparatus and Measuring System

Figure 2 shows an experimental apparatus we constructed in this study. The apparatus consists of water storage section, contraction section and test section. The storage section has a 1.5 m square cross section connected to the contraction section. The contraction section was designed to have parabolic shape to avoid sudden contraction. In the test section with 0.5 m square channel, a circular cylinder with 0.1 m in diameter is assembled.

In the experiments, once a gate is opened, reserved water with volume of about 3 m^3 starts to fall and is accelerated by gravity force. Time variation of measured Reynolds number of the water flow obtained in the current experiment is shown in figure 3. Reynolds number was calculated by bulk velocity of water passing through the test section and the diameter of circular cylinder. It is shown that the flow reaches to highly turbulent flow over critical Reynolds number roughly about $5x10^5$ in 0.5 sec. Henceforth, we call this the high Reynolds number flow. In case of experiments on the intermediate Reynolds number flow (Re=$6x10^4$), we inserted a stainless plate as a flow strainer at the end of the test section. The plate has regularly-arranged holes with 10 mm in diameter to reduce flow velocity.

2.2 Measuring System for particle image velocimetry (PIV)

For measurement of two-dimensional velocity fields on the wake flow formed behind the cylinder, time-resolved particle image velocity (PIV) was applied. In this study, cross-correlation PIV methods originally coded was applied. In the PIV system schematically shown in Fig.2, an Argon-Ion (Ar^+) laser operated at a wavelength of 514.5 nm (Spectra Physics; model 2017; output power: 4 W) was used as a light source. The laser beam was expanded vertically by a series of cylindrical lens for illuminating nylon particles (diameter:30 μm; specific gravity: 1.06) seeded in the water. Time-series behaviour of illuminated particles was monitored by a high-speed CMOS camera (Vision Research; Phantom V5.0). We used an image intensifier (Hamamatsu; C6653) connected to the high-speed camera in an effort to control an exposure time for PIV measurement because the Argon-Ion laser was not a pulse laser, but a continuous wave (CW) laser. The image intensifier was also beneficial to amplify signals from scattered light from the illuminated particle in case of short exposure time adopted. To control timing of exposure on both the CMOS camera and the image intensifier, we used a pulse delay generator (Stanford Research Systems, DG535).

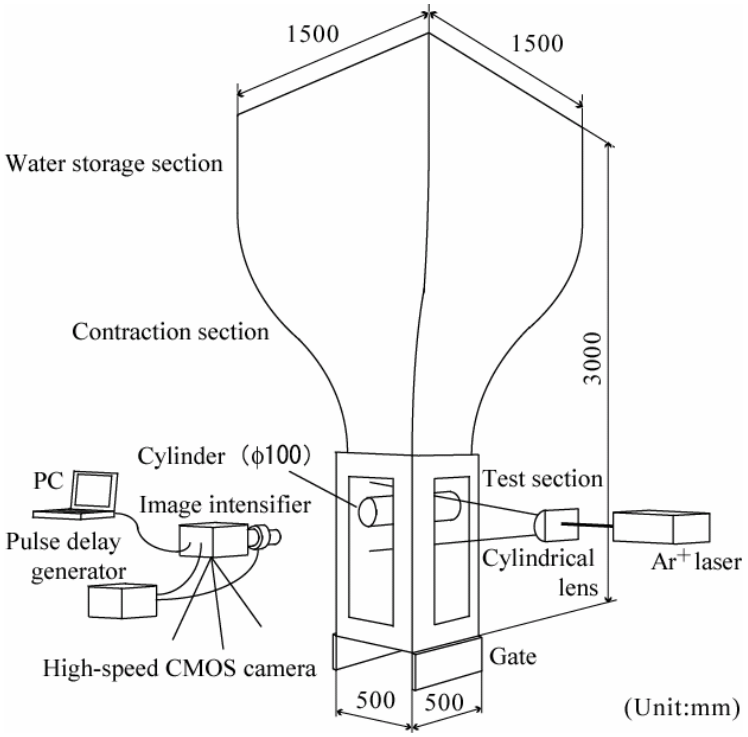

Fig. 2. Experimental apparatus and measuring system for time-resolved particle image velocimetry (PIV)

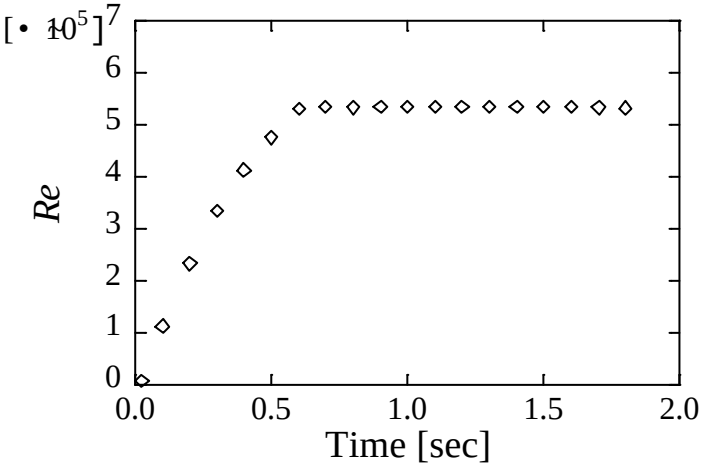

Fig. 3. Time variation of measured Reynolds number after the gate opened in case of the high Reynolds number flow.

3. RESULTS AND DISCUSSION

3.1 Visualisation of the wake flow behind the circular cylinder

A snapshot of the visualised wake flow in case of high Reynolds number (Re=5x10^5) is shown in figure 4a). In the experiment, frame rate of the high-speed CMOS camera was 1000 frames per second and exposure time of the image intensifier was 50 μs. Total 4096 consecutive images were recorded. The image matrix was 512 pixel x 512 pixel, which corresponds to actual area of 330 mm x 330 mm. Not only visualisation around the circular cylinder as displayed in figure 4a), but also visualisation of the downstream up to x/d=5 (x: longitudinal distance from the centre of the cylinder; d: diameter of the cylinder) was conducted. By processing two consecutive images by PIV, we obtained two dimensional velocity fields as depicted in figure 4b).

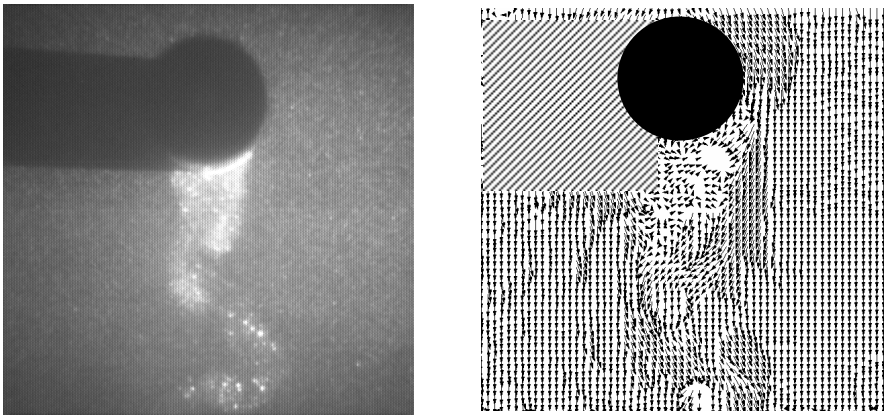

a) *b)*

Fig. 4. Visualisation of the high Reynolds number flow and PIV results around the circular cylinder

a) Visualisation of the flow field. The laser light sheet was introduced from the right side on the image.

b) Instantaneous velocity vectors obtained by PIV.

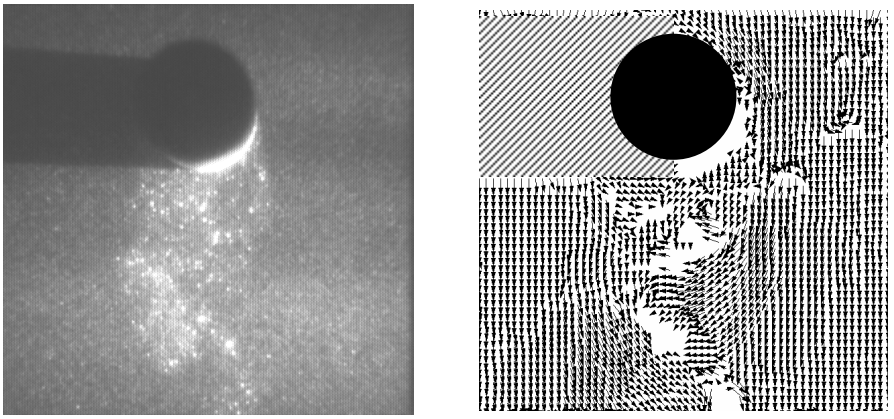

a) *b)*

Fig. 5. Visualisation of the intermediate Reynolds number flow and PIV results around the circular cylinder

a) Visualisation of the flow field. The laser light sheet was introduced from the right side on the image.

b) Instantaneous velocity vectors obtained by PIV.

As shown in figure 4, periodical vortex shedding behind the cylinder was observed. The shed vortices moved downstream with zigzag motion in the turbulent wake flow. It is noteworthy that this vortex marching was packed into the narrow region behind the cylinder in case of the high Reynolds number flow.

On the other hand, in case of the intermediate turbulent flow as shown in figure 5, relatively large vortex and wide zigzag motion of the wake flow was recognised. This distinct difference observed between their flow patterns leads to difference on turbulent properties as discussed in the followings.

3.2 Statistical turbulent properties

To examine turbulent properties of the high Reynolds number flow (Re=5x10^5) in detail, we measured profiles of mean velocity, relative turbulent intensities and Reynolds shear stresses from time-resolved PIV results. Turbulent properties measured at x/d=1.5 are shown in figure 6, in which turbulent properties in case of the intermediate Reynolds number flow (Re=6x10^4) was also plotted for comparison. Note that the mean flow profiles and turbulent properties measured in the intermediate Reynolds number flow are in excellent agreement with experimental results reported by Cantwell et al., 1983, using a hot-wire anemometer.

As shown in figure 6a), the width of wake in case of the high Reynolds number flow (Re=5x10^5) is narrow as much as the cylinder diameter. On the other hand, in the intermediate Reynolds number flow, wake width is twice as much as the cylinder diameter.

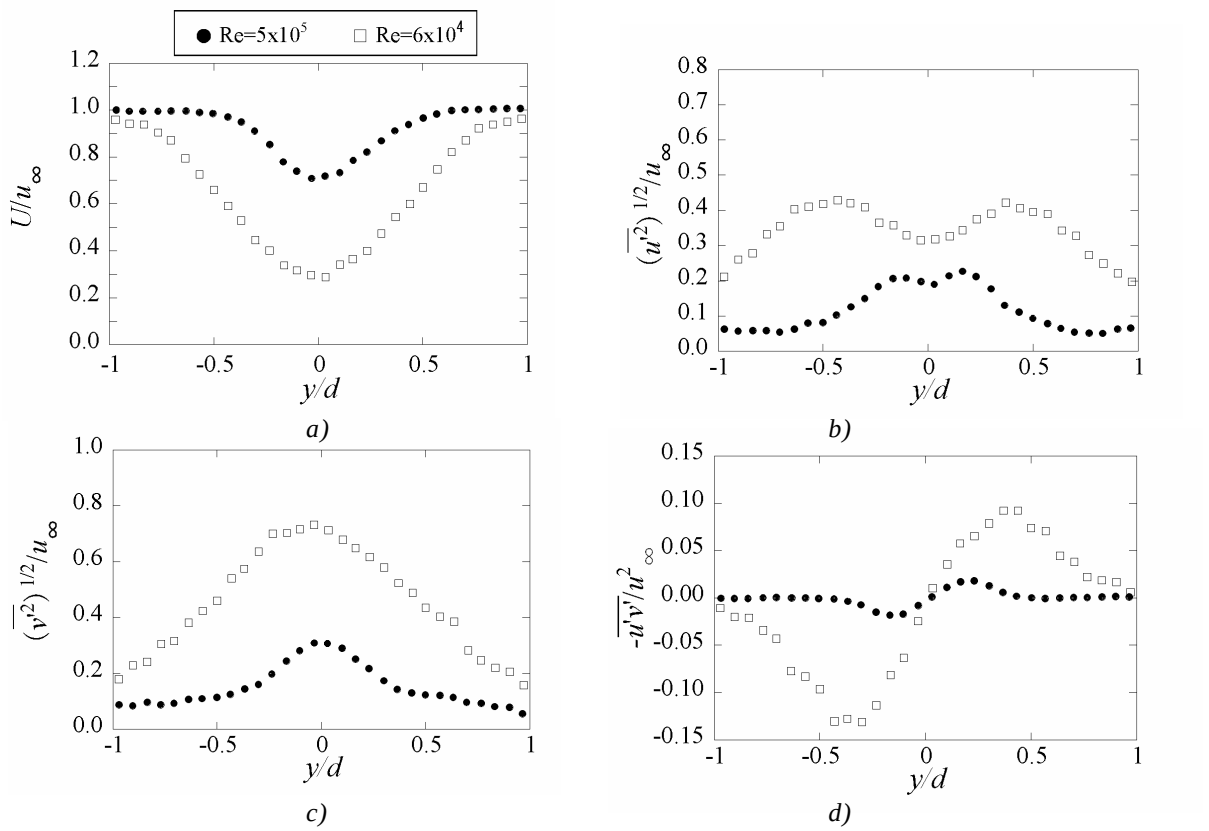

Fig. 6. Turbulent properties measured at x/d=1.5.

a) Mean streamwise velocity.

b) Streamwise turbulent intensities.

c) Lateral turbulent intensities

d) Reynolds shear stresses

Turbulent intensities normalised by free stream velocity, u_δ, was also very distinctive as shown in figure 6b) and figure 6c). Relative turbulent intensities in case of the high Reynolds number are smaller than that in the intermediate Reynolds number flow in both streamwise and lateral direction. Comparing the turbulent intensities in both flows, the maximum intensity in the high Reynolds number flow shows one half to that in the intermediate Reynolds number flow. It is also shown in figure 6d) that normalised Reynolds shear stresses are one half in the high Reynolds number flow to that in the intermediate Reynolds number flow.

These differences on turbulent properties between the high and the intermediate Reynolds number flows must be explained on vortex structure formed behind the cylinder. Flow visualisation result in figure 4 and figure 5 clearly shows that size of vortex and zigzag motion of the wake flow is distinctively different each other. In case of the high Reynolds number flow, vortex marching is limited to narrow region behind the cylinder and vortex size seems to be small compared to the one in the intermediate Reynolds number flow.

Figure 7 shows time variation of lateral flow velocity measured at x/d=1.5, y/d=0.24 in case of the high Reynolds number flow (figure 7a)). Lateral flow velocities at x/d=1.5, y/d=0.55 in case of the intermediate Reynolds number flow was also shown in figure 7b). Periodic behaviour of fluctuation was observed in both flows. This corresponds to experimental observation of alternative vortex shedding behind the cylinder in figure 4 and figure 5. Strouhal number, St, representing normalised vortex shedding frequency, was defined as the following equation,

$$St = fd / u_\infty ,$$

where f is measured vortex shedding frequency, d is a diameter of the cylinder and u_δ is free stream velocity. In case of the high Reynolds number flow, Strouhal number, St, is about 0.55, while 0.19 in case of the intermediate Reynolds number flow. Thus, normalised vortex shedding frequency in the high Reynolds number wake flow was higher than that in the intermediate one. Judging from the flow visualisation in figure 4 and figure 5, vortices in the high Reynolds number flow is rather small, but vortex shedding more frequently occurred behind the cylinder, according to Strouhal number deduced. Adding to that, flow entrainment by vortex also seems to be small in the case of the high Reynolds number flow. This results in reduction of turbulent fluctuation behind the cylinder and thus suppression of turbulent intensities measured in figure 6.

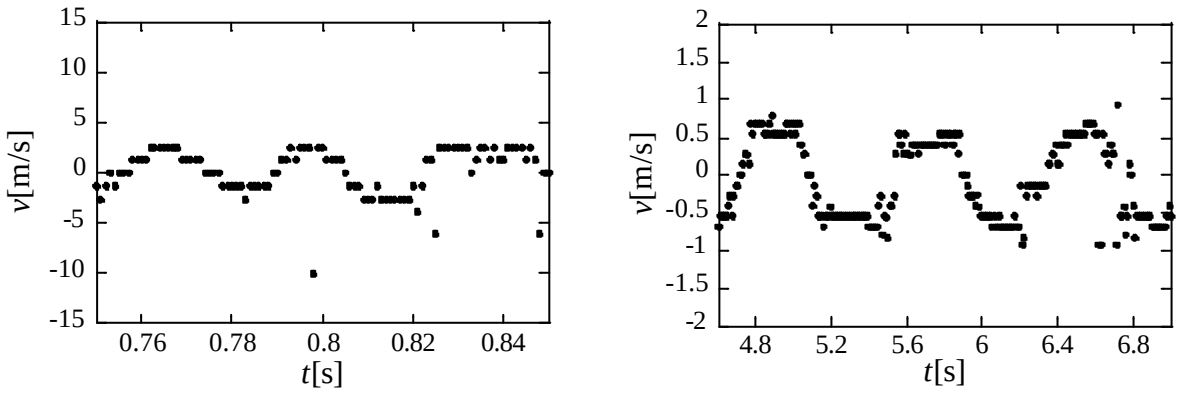

a) *b)*

Fig. 7. Time variation of lateral flow velocity. Note that time scale is in difference in both plots.

a) The high Reynolds number flow. Measured at x/d=1.5, y/d=0.24.

b) The intermediate Reynolds number flow. Measured at x/d=1.5, y/d=0.55.

4. SUMMARY

Toward the implementation of CO_2 ocean sequestration, turbulent flow fields behind the cylinder was examined by applying flow visualisation and time-resolved PIV measurement to the laboratory-scaled experimental apparatus creating the high Reynolds number flows (Re=5x10^5). We succeeded in measuring turbulent motion and its properties in the high Reynolds number flow over the critical Reynolds number, which will contribute for a numerical simulation of turbulent

flow field and dispersion process of released CO_2 in the ocean. We also conducted the flow field measurement with the intermediate Reynolds number (Re=6x10^4) for comparison. It was revealed that wake width in the case of the high Reynolds number flow was as half as the one in the intermediate Reynolds number flow. The turbulent intensities and Reynolds shear stresses in the high Reynolds number flow were about a half of those measured in the intermediate flow. These distinctive differences observed each flow was caused by vortex structure generated behind the cylinder. The results on flow field visualisation suggested that vortex marching was restricted in rather narrow region in case of the high Reynolds number flow. It was also found that the vortex shedding frequency was small in case of the high Reynolds number flow. This results in reduction of turbulent fluctuation behind the cylinder and thus suppression of turbulent intensities in the high Reynolds number flow.

ACKNOWLEDGEMENT

The authors would like to acknowledge the courtesy of Prof. T. Miyauchi and Prof. M. Tanahashi in Tokyo Institute of Technology for arrangement of utilisation of an Ar-Ion Laser used in this study. We also show our gratitude to Prof. I. Satoh and T. Saitoh in Tokyo Institute of Technology for their support on experiments. Financial support by RITE (Research Institute of Innovative Technology for the Earth) and NEDO (New Energy and Industrial Technological Development Organization) was also acknowledged.

REFERENCES

Cantwell, B. and Coles, D. (1983), "An Experimental Study of Entrainment and Transport in the Turbulent near Wake of a Circuler Cylinder", *J. Fluid Mech.*, 136, pp.321-374.

Chen, B., Song, Y., Nishio, M., Akai, M. and Ohsumi, T. (2003), "A Hybrid Numerical Model of LCO_2 and CO_2 Enriched Seawater Dynamics in the Ocean Induced by Moving-Ship Releasing", *Greenhouse Gas Control Technologies*, 1, pp.771-776.

Liro, C. R., Adams, E. E. and Herzong, H. J. (1992), "Modeling the Release of CO_2 in the Deep Ocean", *Energy Convers. Mgmt*., 33(5-8), pp.667-674.

Marchetti, C. (1997), "On Geoengineering and the CO_2 problem", *Climate Change*, 1, pp.59-68.

Morishita, M., Cole, K. H., Stegen, G. R. and Shibuya, H. (1993), "Dissolution and Dispersion of a Carbon Dioxide Jet in the Deep Ocean", *Energy Convers. Mgmt*., 34(9-11), pp.841-847.

Murai, S., Ohsumi, T., Nishibori, F. and Ozaki, M. (2003), "The Second Phase of Japanese R&D Program for CO_2 Ocean Sequestration, *Greenhouse Gas Control Technologies*, 1, pp.733-738.